Effect of the thermal quench on aging in spin glasses

G. F. Rodriguez,[1] G. G. Kenning,[2] and R. Orbach[3]
[1]*Department of Physics, University of California, Riverside, California 92521-0101, USA*
[2]*Department of Physics, Indiana University of Pennsylvania Indiana, Pennsylvania 15705-1098, USA*
[3]*Department of Mechanical Engineering, The University of Texas at Austin, Austin, Texas 78712, USA*
(Received 8 May 2013; published 9 August 2013)

We probe the effects of different initial conditions on the process of aging in spin glasses arising from alternative temperature quenching protocols for the canonical and representative Cu:Mn (6 at.%) dilute magnetic alloy. The effects of these changes are observed through the decay of the thermoremanent magnetization, $M_{\rm TRM}(t)$. We find significant changes in the initial state as a consequence of the different cooling processes, reflected through an effective waiting time, $t_w^{\rm eff}$. The effective waiting time shortens as the time spent above the measuring temperature in the cooling protocol is reduced, reaching a minimum when the temperature is not allowed to rise above the final measurement temperature after the initial quench. This behavior is consistent with the picture of a rapid temperature dependence of the barrier heights separating metastable states.

DOI: 10.1103/PhysRevB.88.054302 PACS number(s): 75.50.Lk, 75.10.Nr, 75.78.−n, 75.60.Ej

I. INTRODUCTION

Measurements of the dynamic response of the spin glass state provide insights into the nature of the spin glass phase, while at the same time presenting an experimental challenge still not fully explored or understood. The spin glass phase was first observed as a cusp in the ac magnetic susceptibility of the dilute alloy AuFe, by Cannella and Mydosh.[1] The cusp was found to be time dependent[2] providing the first of many interesting time-dependent effects in these materials. Analysis of this time dependence shows a temperature variation of the cusp as a function of ac frequency, spanning all measurement time scales. Extensive measurements have been performed in bulk samples to ascertain whether the time-dependent cusp represents a glasslike transition, or could be extrapolated (at infinite time scale) to a finite transition temperature, implying a phase transition.[3]

The cusp also marked the onset of remanent behavior. Upon cooling the spin glass sample from high temperature in a constant magnetic field, the magnetization initially follows a Curie-Weiss-like behavior. Cooling the spin glass further, through the cusp temperature, the magnetization remains approximately constant at a value $M_{\rm FC}$ (although a weak logarithmic decay as a function of time has been observed[4]). This is an indication that the spins are frozen in random directions with a net bias $M_{\rm FC}$ because of the applied field.

Upon subsequent removal of the magnetic field, there is a rapid (reversible) decrease in the sample magnetization, from $M_{\rm FC}$ to $M_{\rm FC} - M_{\rm ZFC}$. $M_{\rm ZFC}$ is the value of the sample magnetization obtained when cooled in zero magnetic field to the measurement temperature and the same magnetic field is applied. This difference is called the thermoremanent magnetization $M_{\rm TRM}(t)$, observed to be time dependent, and diminishing (in principle) to zero for very long times. The remarkable property of spin glasses is that the decay of $M_{\rm TRM}(t)$ depends upon the time spent from passage through the cusp temperature to when the applied field is removed at the measurement temperature, even though $M_{\rm FC}$ appears to be more or less constant. This is referred to as the aging process, where the time spent in the magnetic field at the measurement temperature T_m is referred to as the waiting time, t_w.

Various measurements, including ac susceptibility,[5] dc magnetization,[6] muon decay,[7] neutron spin echo,[8] and NMR,[9] provide evidence that the rapid part of the decay (from $M_{\rm FC}$ to $M_{\rm FC} - M_{\rm ZFC}$) is power law in nature. The power-law term is independent of the waiting time t_w, and is termed the stationary term (i.e., stationary with respect to the waiting time t_w).

Between 1982–84, experiments by several groups first observed the time dependence of the thermoremanent magnetization, $M_{\rm TRM}(t,t_w)$, in spin glasses.[10,11] In these measurements, the sample is cooled in a small constant magnetic field through the cusp temperature (now referred to as the spin glass transition temperature, T_g) to a measuring temperature $T_m < T_g$. After waiting a time t_w in the presence of the magnetic field, the field is rapidly removed and the consequent magnetization decay of the sample is measured. The time dependence of the remanent magnetization, $M_{\rm TRM}(t,t_w)$, is weak and very slow, posing substantial experimental challenges. The advent of superconducting quantum interference device (SQUID) technology made the weak signals accessible, but the thermal and vibrational requirements of measurements over long times require care.

The dependence of the magnetization decay on t_w is termed aging. Analysis of early data found that the structure of the shorter time components of this decay could be fitted to a power law plus a stretched exponential.[6,10] Extending this analysis, Nordblad *et al.*[12] found that, in the short time region ($t < t_w$), the decay was composed of three additive terms: a weak field-dependent power-law term, a power-law term and a waiting-time-dependent term, which included a stretched exponential form. Subsequent measurements[13] of the remanent magnetization decay to longer times than the early experiments found an inflection point in the decay (at a time approximately equal to t_w), leading to a breakdown of the stretched exponential analysis. Two techniques were then developed for analyzing the decay functions. The first technique was derived from the inflection point. Taking the logarithmic derivative $S(t) = dM_{\rm TRM}(t,t_w)/d\ln t$ of the decay leads to a peak in $S(t)$ at a time approximating the waiting time t_w. This has the physical meaning of a characteristic time for

the spin glass decay, and as we shall see, is a useful measure of the effect of differing cooling protocols. We shall term $S(t)$ the relaxation function.

The second technique developed for analyzing the spin glass time decay of $M_{\rm TRM}(t,t_w)$ relies on a parametrization of time in analogy with the strain creep of glassy polymers and other disordered compounds (see Struik[14]). The Saclay group[5,15–17] extended this analysis to spin glasses, using a multiplicative ansatz,

$$M_{\rm TRM}(t,t_w) \propto t^{-\alpha} F(t_e/t_w^{\mu}), \tag{1}$$

where the "effective time" t_e is introduced and μ is an empirical fitting parameter. The age of the system increases with the observation time $t_w + t$, so that the time/age ratio decreases. In order to describe the relaxation by the same t_w, the effective time t_e should increase more slowly than the observation time. This means that $dt_e/t_w = dt/(t + t_w)$. This would imply that $M_{\rm TRM}(t,t_w)$ would scale as t/t_w, contrary to observation.[15–17] In order to account for this deviation, they introduced the parameter μ such that

$$dt_e/t_w^{\mu} = dt/(t + t_w)^{\mu}, \tag{2}$$

so that an effective time is given by

$$t_e = t_w[(1 + t/t_w)^{1-\mu} - 1]/(1 - \mu), \tag{3}$$

where $\mu = 1$ is the limit for perfect scaling [i.e., $M_{\rm TRM}(t/t_w)$ scales as t/t_w].

Alba *et al.*[17] found that the $M_{\rm TRM}(t,t_w)$ decay curves, as a function of t_e rather than t, reduces them to a unique master curve. The exponent μ is itself a function of temperature. Values range [see inset of Fig. 2 in Ref. 16] from a low of $\mu \approx 0.7$ at $T/T_g = 0.3$ to a maximum of $\mu \approx 0.9$ at $T/T_g = 0.8$, then falling sharply back to $\mu \approx 0.7$ in the vicinity of T_g.

It was Zotev *et al.*[18] who demonstrated that μ depended on the initial preparation of the system. They introduced the concept of the ZTRM, the decay of $M_{\rm TRM}(t,t_w)$ at $t_w = 0$, and showed that μ depended upon the cooling protocol to reach the final measurement temperature at which the magnetic field was removed. It was known that the details of the experimental protocol well above the measurement temperature T_m do not affect the measured relaxation properties.[19] However, Zotev *et al.*[18] displayed a strong impact of observed spin glass behavior on the thermal history in the immediate vicinity of T_m, for $T = T_m + \Delta T$ such that $\Delta T < 0.5$ K. This independent observation is in remarkable accordance with the temperature interval over which the barrier heights in the barrier model were observed to diverge.[20]

We suggest that the dependence of μ on the cooling protocol in the vicinity of the measurement temperature T_m is a consequence of diffusion between accessible states in free energy phase space. This effect is manifest through the extraction of an "effective waiting time," $t_w^{\rm eff}$, as derived from the position of the peak in $S(t) = dM_{\rm TRM}(t)/d\ln t$. Rodriguez *et al.*[21] demonstrated for Cu:Mn (6 at.%) that the more rapid the cooling to T_m in a temperature regime close to T_m, the shorter $t_w^{\rm eff}$, and the closer μ approaches unity (see Fig. 1 in Ref. 21). They also showed that the nature of the cooling protocol matters: the longer the sample temperature was above but close to T_m during cooling, the larger became $t_w^{\rm eff}$, and the smaller became μ. Finally, for very rapid cooling where the temperature is not allowed to rise above T_m in the close vicinity of T_m, they showed $t_w^{\rm eff}$ could be made very short (19 s) and $\mu = 0.999$.

A second model that has evolved to explain aging effects, and in particular the "end of aging"[22] in spin glasses, begins with a heterogeneous initial state.[23,24] The starting point for this model proposes that the spin glass sample is composed of many spin glass domains which form at the transition temperature. The starting point for systems far from equilibrium usually requires that the initial occupancy of phase space be far from the equilibrium distribution, and for long-time dynamics, separated by large energy barriers. It is generally accepted, whether one looks at the mean field Parisi solution to the Sherrington-Kirkpatrick model,[3] the real-space droplet model,[25] dynamic experimental properties of spin glasses,[20] or numerical studies of Edward-Anderson spin glasses,[26] that the energy barrier space is hierarchical with diffusion time scales (for theoretical models) spanning an infinite range. To this general concept was added the conjecture that the system is an ensemble averaged over many initial states, each starting from different positions within the hierarchy of barriers. This is equivalent to a spatial heterogeneity with each domain having a different effective fluctuation time scale with times spanning the whole range of possible time scales. The concept of spatial heterogeneity with a distribution of time scales is not new to aging dynamics.[27] In spin glasses, Chamberlin[28] observed nonresonant spectral hole burning in a AuFe (5%), which he attributes to a distribution of relaxation times corresponding to a heterogeneous system composed of many domains, each with its own characteristic temporal behavior. This heterogeneity of time scales conjecture is reasonable as the thermal quench in spin glasses is a complicated, nonequilibrium, process with a particular realization evolving (below the transition temperature) through a very rapidly growing barrier space. The realization has very little equilibration time, leading to a no *a priori* basis for occupation of any particular state. This model has been used to provide explanations for the long-time logarithmic decay, and the the temperature dependence of the scaling parameter μ, within the context of aging materials.

Other studies on the effects of the cooling protocol have been reported by Refregier *et al.*[19] Djurberg *et al.*[4] measured the aging of the zero field cooled and field cooled analogy of ZTRM. Their pioneering work noted that "the behavior for positive ΔT does not give the perfect overlap with the corresponding response attained at T_m that a negative ΔT gives." This is of course quite consistent with our own analysis.

To make contact with previous scaling analyses,[15–17] we separate the decay of $M_{\rm TRM}(t,t_w)$ into an additive stationary decay term, and an aging part of the decay of $M_{\rm TRM}(t,t_w)$:

$$M_{\rm TRM}(t,t_w) = M_{st}(t) + M_{\rm aging}\left(t/t_w^{\mu}\right). \tag{4}$$

The stationary term depends upon time as a power law, independent of t_w. It dominates at short measuring times, $t \ll t_w$, and can be written as

$$M_{st} = At^{-\alpha} t \ll t_w. \tag{5}$$

Refrigier *et al.*[19] determined the constant A and the exponent α for the insulating spin glass $CdCr_{1.7}In_{0.3}Sr$ using

measurements of the out-of-phase component of the ac susceptibility at $\nu = 10^{-2}$ Hz. A value of $A \approx 1$ was observed with the power $\alpha \approx 0.02$. Vincent *et al.*[29] proposed that, in general, the stationary term should be subtracted before scaling. As an example, for the spin glass Ag:Mn, they found that subtraction of the stationary term changes μ from 0.87 to 0.97.

In this report, we expand upon the results of Rodriguez *et al.*[21] through a detailed examination of the relationship between the cooling protocol and the initial conditions of the canonical and representative Cu:Mn (6 at.%) spin glass, defined as the state of the spin glass at the time that the magnetic field is removed. We separate the protocols into "no undershoot" (the temperature never drops below the final measuring temperature T_m during the cooling to T_m), the "conventional or commercial protocol" (where the temperature drops below T_m, then oscillates in the vicinity of T_m, rising above and below before finally settling to T_m), and "no overshoot" (the temperature never rises above the measuring temperature T_m during the cooling approach to T_m after the initial quench).

II. THE TEMPERATURE QUENCH AND INITIAL CONDITIONS

Spin glass dynamics are known to depend on the initial preparation conditions.[18] The initial conditions are defined as "the state of the sample at the time the sample reaches its measuring temperature T_m after a thermal quench from above the spin glass transition temperature T_g, and just before the magnetic field is removed." To date, a detailed examination of the role of the initial conditions on aging dynamics has not been systematically investigated. A series of cooling protocols are developed in this section in order to probe, in a reasonably systematic manner, differing initial conditions and their effects on the decay of $M_{\rm TRM}(t,t_w)$.

Our construction of cooling protocols relies on several important experiments. The first is the temperature cycling experiments by Refregier *et al.*[19] They found that small positive increases in temperature during the waiting time and above the measuring temperature, T_m, increased the aging rate, while large positive increases erased the memory of the preceding cooling protocol. Small negative decreases in temperature decreased the aging rate, and large negative temperature shifts "froze" the system with no aging. Lederman *et al.*[20] showed that within a small temperature interval $\Delta T \leqslant 80$ mK around the aging measurement temperature, [Ag:Mn (2.6 at.%), $T_m = 9$ K, $T_g = 10.4$ K], aging decreases reversibly for negative temperature shifts while aging increases reversibly for positive temperature shifts. Above this temperature interval, the decay curves do not return to those at the measuring temperature upon cycling. This is a result of a *combination* of the normal continuation of phase-space exploration at T_m and a re-equilibrium within the subspace populated while waiting in a field at $T_m \pm \Delta T$. We shall argue that it is precisely this combination through the cooling protocol that results in $\mu < 1$. The temperature profile therefore needs to be controlled and observed through a sufficiently small temperature range $T_m \pm \Delta T$ that preserves the reversibility for aging of the system. Our cooling protocols carefully control the temperature (and range) in the regime $T_m \pm \Delta T$. The magnitude of ΔT is material dependent. For our sample [Cu:Mn (6 at.%), $T_m = 26$ K, $T_g = 31.5$ K], we have determined $\Delta T \approx 300$ mK.

Six cooling protocols are exhibited in this report that demonstrate the effects of the initial state upon the scaling properties of $M_{\rm TRM}(t,t_w)$. The cooling process and the initial state are initially characterized through an effective "cooling time," $t_c^{\rm eff}$ extracted from the position of the peak of the zero waiting time ZTRM relaxation function $S(t) = dM_{\rm ZTRM}(t)/d\ln t$ as a function of $\ln t$. The six different cooling protocols will each have an actual cooling time, t_c, to arrive at T_m, and, depending on the protocol, an effective cooling time $t_c^{\rm eff}$ deduced from the peak of $S(t) = dM_{\rm ZTRM}(t)/d\ln t$. The very nature of the cooling protocols (finite time to reach T_m) will mean that in general $t_c^{\rm eff} > t_c$.

All the experiments were performed using a home-built dc SQUID magnetometer, with the cooling protocols repeated several times to check for reproducibility. Helium gas is used as the median for heat transfer between the liquid helium bath and sample, with the cooling rate controlled by the amount of helium gas. Using the amplified output from a Cryogenics potentiometer bridge to control the temperature, we obtained a temperature stability at the measuring temperature $T_m = 26\,{\rm K} \pm 5$ mK for up to 100 000 s. We enclosed the 9-T magnet surrounding the sample space with 4-mm-thick superconducting Pb plating. The shielding was continued approximately 70 cm up the sample insertion rod to minimize noise. The superconducting shield greatly reduced the ambient noise in the system. The combination of shielding plus a new dc SQUID amplifier gave a sensitivity of approximately 2–3 orders of magnitude greater than previous versions of our system. Measurements were taken every 0.3 s from 2 s up to 50 s, and then every three seconds thereafter. This yielded several thousand data points for the shortest runs, and ten of thousands of data points for the longest runs. The small magnetization decay of the sample chamber itself was measured and found to be reproducible. It was subtracted from all of the data sets. The sample used in the study is the previously characterized[30] metallic spin glass Cu:Mn (6 at.%).

For each of the cooling protocols described in the next section, a series of TRM decay measurements were performed with waiting times of $t_w = 50$, 100, 300, 630, 1000, 3600, 6310, and 10 000 s. The transition temperature of 31.5 K was determined from the onset of remanence, and all of the experiments were measured at $T = 26$ K ($T_m/T_g = 0.83$). All cooling protocols began from a temperature of 35 K. The applied field was 20 G. The waiting time clock began at the end of the cooling protocol when the temperature was determined to be stable at the measuring temperature T_m. Most of the cooling protocols used a cooling rate of 0.6 K/s. The fast cooling protocol was 1.0 K/s.

A. 406-s effective cooling time protocol 1—no undershoot version 1 (NUS1)

Commercial SQUID magnetometers are known to have rather long cooling times, as much as 500 s depending on the

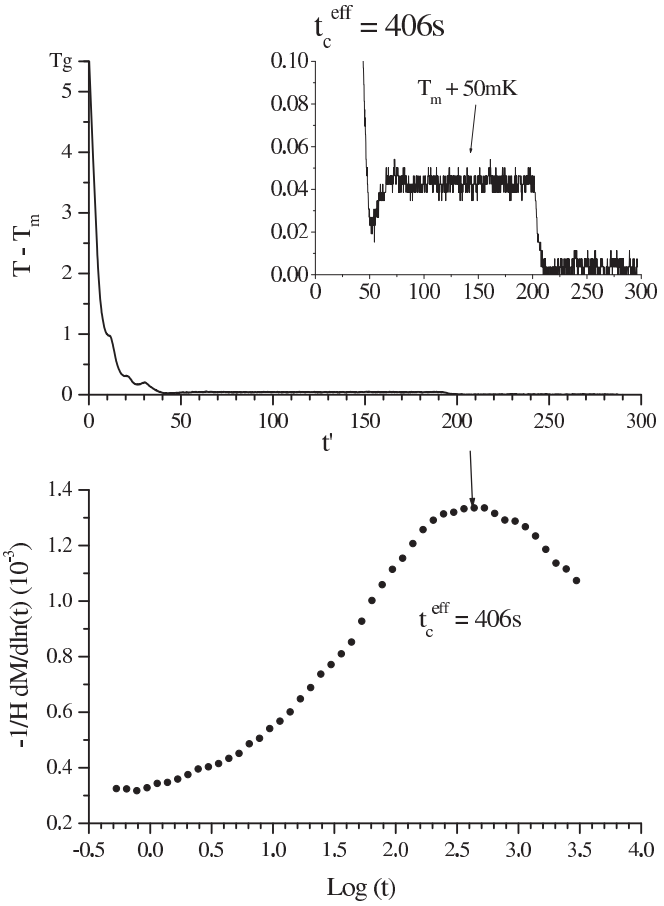

FIG. 1. NUS1 cooling protocol. This protocol is used to increase the cooling time to times comparable with commercial machines. The initial cooling rate is 0.6 K/s. The approach to T_m is from above. The temperature was held at an intermediate temperature, $T' = 50$ mK + T_m. The insert in the upper figure shows the time spent at T' and time at T_m. The lower figure is the relaxation function for this cooling protocol, from which $t_c^{\text{eff}} = 406$ s is extracted.

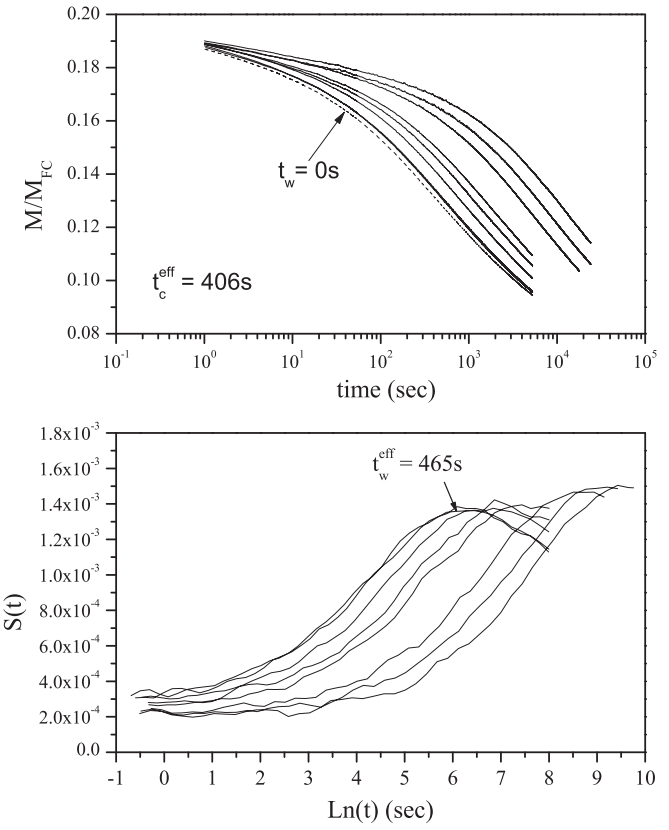

FIG. 2. $M_{\text{TRM}}(t,t_w)$ decays for the NUS1 cooling protocol. The curves are for t_w 50, 100, 300, 630, 1000, 3600, 6310, and 10 000 s, respectively. The uppermost magnetization curve has the longest waiting time, and the decay curves systematically decrease in magnitude as the waiting time decreases. The lowest decay curve (dashed line) is the ZTRM ($t_w = 0$ s). The lower figure displays the $S(t)$ relaxation functions for the $M_{\text{TRM}}(t,t_w)$ curves. The effective time $t_w^{\text{eff}} = 465$ s is extracted from the maximum of the $S(t)$ relaxation function for $t_w = 50$ s.

measuring temperature.[18] One of the major advantages of our apparatus is that we determine when the temperature is stable in real time, and end the cooling process manually. NUS1 increases the effective cooling time to a value comparable to those reported for commercial SQUID magnetometers. The cooling protocol is shown in the upper curve of Fig. 1, taking advantage of the fact that aging is faster at temperatures slightly above T_m.

The temperature is first lowered in this protocol to an intermediate temperature (T') 50 milli-Kelvin above the final measuring temperature, $T' = 50$ mK + T_m, taking about 50 s. The temperature is held at T' for about 150 s (insert of Fig. 1). The temperature is then lowered to T_m where another 100 s is taken for temperature stability. The actual time for cooling is $t_c = 300$ s. The effective cooling time determined from $S(t)$ in Fig. 1 is $t_c^{\text{eff}} = 406$ s.

A series of TRM experiments are performed using this cooling protocol. The waiting times span the time range $t_w = 50$–10 000 s. The waiting time clock started after the cooling protocol had ended. The magnetization decay curves are plotted in the upper graph of Fig. 2. The lower graph of Fig. 2 are the relaxation functions $S(t)$ for the $M_{\text{TRM}}(t,t_w)$ curves.

B. 143-s effective cooling time protocol 2—no undershoot version 2 (NUS2)

In this protocol, NUS2, the temperature does not fall below T_m for the entire time of the cooling protocol, illustrated in the upper curve of Fig. 3. The cooling time t_c is 90 s; the time spent in the ΔT region is 50 s. The effective cooling time is extracted from the position of the peak in the relaxation function $S(t)$ and found to be $t_c^{\text{eff}} = 143$ s.

The $M_{\text{TRM}}(t,t_w)$ decay experiments for the NUS2 cooling protocol were performed for waiting times t_w from 50 to 10 000 s. The waiting time clock began when the cooling protocol ended. The decays are plotted in the upper graph of Fig. 4. The lower graph in Fig. 4 displays the $S(t)$ relaxation function for the $M_{\text{TRM}}(t,t_w)$ curves. It is seen, for example, that for $t_w = 50$ s, $t_w^{\text{eff}} = 251$ s, showing that the effective waiting time is not just the addition of the effective cooling time, t_c^{eff} plus the actual waiting time, t_w, but in general well in excess of their sum. This will be discussed further in Sec. III.

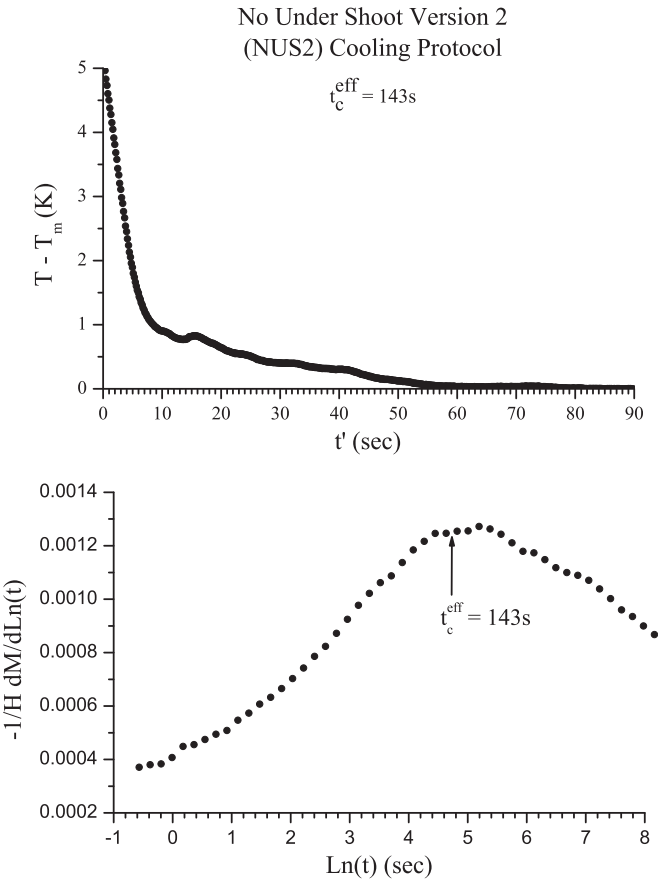

FIG. 3. NUS2 cooling protocol. The cooling rate is 0.6 K/s. The approach to T_m is from above. The cooling rate is decreased when the temperature is within 1K of T_m. The cooling time is about 90 s. The lower graph is the $S(t)$ relaxation function for this cooling protocol, from which $t_c^{\rm eff} = 143$ s is extracted. $S(t)$ is much broader in the first two cooling protocols, as compared to the subsequent protocols.

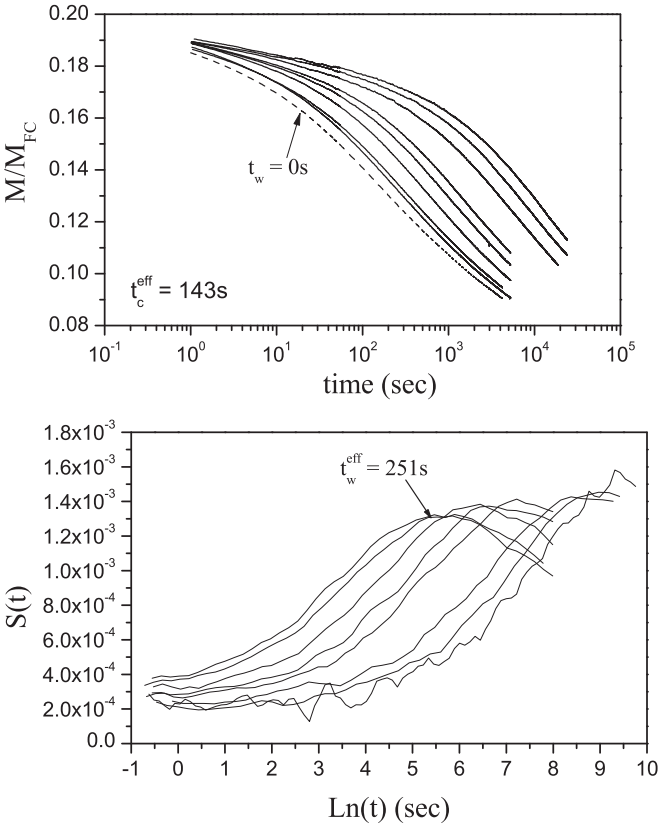

FIG. 4. $M_{\rm TRM}(t,t_w)$ decays for the NUS2 cooling protocol. The curves are for t_w: 50, 100, 300, 630, 1000, 3600, 6310, and 10 000 s, respectively. The uppermost magnetization curve has the longest waiting time, and the decay curves systematically decrease in magnitude as the waiting time decreases. The lowest decay curve (dashed line) is the ZTRM ($t_w = 0$ s). The lower figure displays the $S(t)$ relaxation functions for the $M_{\rm TRM}(t,t_w)$ curves. The effective time $t_w^{\rm eff} = 251$ s is extracted from the maximum of the $S(t)$ relaxation function for $t_w = 50$ s.

C. 105-s effective cooling time protocol 3—no undershoot version 3 (NUS3)

A third version of the "no undershoot" protocol, NUS3, (see Fig. 5) is a slight misnomer because there is a small undershoot. However, its magnitude is so much less than $\Delta T = 300$ mK that no effect should follow from the undershoot. Following the work of Refregier *et al.*[19] and Hammann *et al.*,[20] the NUS3 protocol probes the effects of aging at temperatures much greater than $\Delta T \approx 300$ mK above the measuring temperature. The NUS2 protocol is repeated in NUS3, but at an intermediate temperature well above $T_m + \Delta T$, so that aging should depend only on the time it takes to go from the intermediate temperature to T_m. This differs from protocol NUS2 in that NUS2 depends on the entire cooling protocol.

In protocol NUS3, the temperature is first lowered to an intermediate temperature T' 3 K above the measuring temperature: $T' = T_m + 3$ K. The temperature is held for 200 s at T', before it is lowered to the final measuring temperature T_m in the "conventional manner" (see Sec. II D). The total time for protocol NUS3 is about 300 s. The time spent in the temperature region of interest, ΔT, during the second temperature shift is ≈80 s, of which 20 s are spent above T_m. The maximum overshoot during the second time interval is 100 mK.

The effective cooling time $t_c^{\rm eff} = 105$ s of the NUS3 cooling protocol is extracted from the relaxation function, $S(t)$, exhibited in the lower graph in Fig. 5. The $M_{\rm TRM}(t,t_w)$ decay curves are plotted in Fig. 6. The lower graphs in Fig. 6 are the relaxation functions $S(t)S(t)$ for the $M_{\rm TRM}(t,t_w)$ curves. For $t_w = 50$ s, the effective time $t_w^{\rm eff} = 177$ s.

D. 73-s effective cooling time protocol 4—conventional cooling protocol (CCP)

Most commercial magnetometers use a feedback loop to control and stabilize the temperature, mimicking a damped harmonic oscillator. Such a cooling protocol will be termed "conventional." Without computer controlled intervention, the approach of our temperature controller to the measuring temperature T_m would also be a damped oscillator (upper part of Fig. 7).

Temperature controls in commercial SQUID magnetometers are designed to cover large temperature ranges for a wide variety of applications, so that quickly reaching a desired measuring temperature is not usually a system priority.

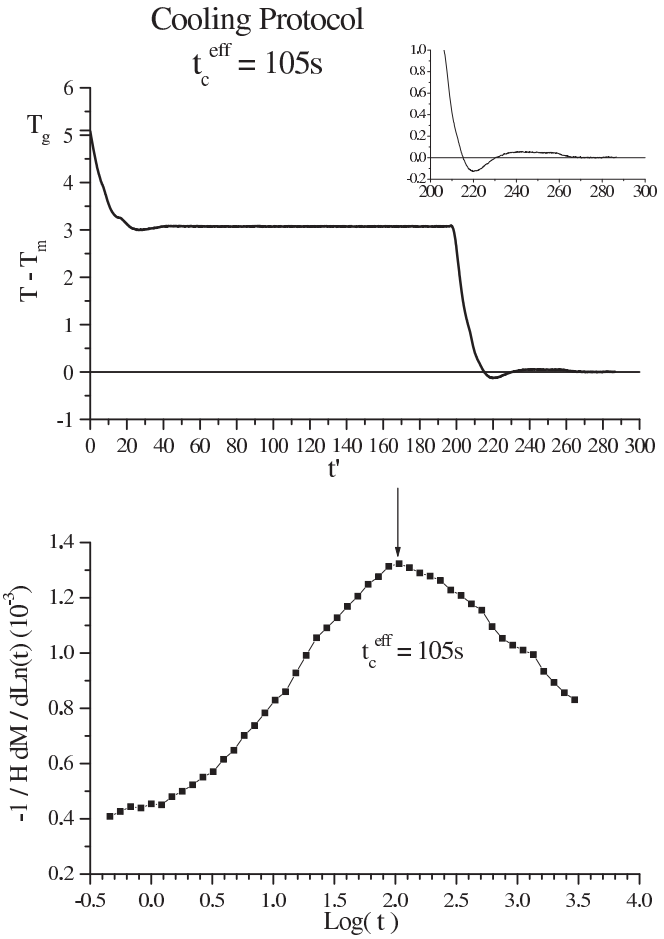

FIG. 5. NUS3 cooling protocol. This protocol is designed to show that aging at a sufficiently higher temperature does not effect aging at the measurement temperature. The cooling rate is 0.6 K/s. In the upper figure, the t' clock starts when T_g is crossed. The intermediate temperature is $T' = 3\ \mathrm{K} + T_m$. The final approach to T_m is the "conventional" damped oscillation approach. The lower graph is the $S(t)$ relaxation function for this cooling protocol from which $t_c^{\mathrm{eff}} = 105$ s is extracted.

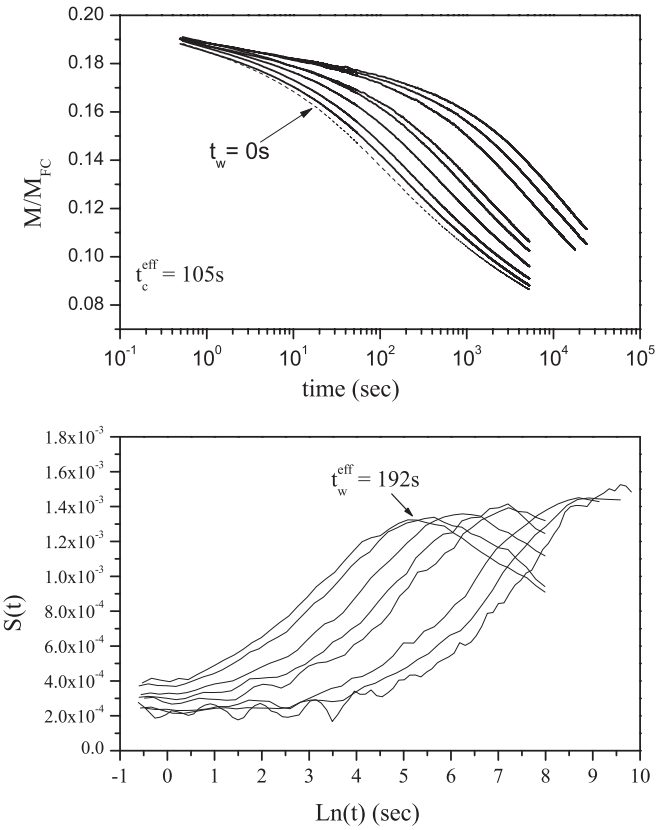

FIG. 6. $M_{\mathrm{TRM}}(t,t_w)$ decays for the NUS3 cooling protocol. The curves are for t_w 50, 100, 300, 630, 1000, 3600, 6310, and 10 000 s, respectively. The uppermost magnetization curve has the longest waiting time, and the decay curves systematically decrease in magnitude as the waiting time decreases. The lowest decay curve (dashed line) is the ZTRM ($t_w = 0$ s). The lower figure displays the $S(t)$ relaxation functions for the $M_{\mathrm{TRM}}(t,t_w)$ curves. The effective time $t_w^{\mathrm{eff}} = 177$ s is extracted from the maximum of the $S(t)$ relaxation function for $t_w = 50$ s. The effective waiting time of the curves is larger than the waiting time plus the cooling time, i.e., $t_w^{\mathrm{eff}} > t_w + t_c^{\mathrm{eff}}$.

Removal of the applied field in a TRM experiment takes place after temperature stability is achieved, so that the time taken for the temperature to stabilize is not usually considered in a TRM scaling analysis. Further, temperature oscillations around the final measuring temperature T_m may have a profound effect on the memory of the system. Negative ΔT can freeze aging, while positive ΔT can accelerate aging, and for sufficiently large excursion, can erase memory altogether.[19] This means that an uncontrolled thermal history approaching T_m could have a significant effect on the effective age of the system.

In order to investigate this question, the temperature is controlled in this section by our controller through a programmed sequence that we designate as the conventional cooling protocol (CCP). The temperature is lowered to below the measuring temperature T_m at a rate of 0.6 K/s, then a damped oscillation around T_m takes place until the control system determines the temperature is stable at T_m. The initial undershoot is found to be ≈2 K below T_m, followed by an overshoot of ≈80 mK above T_m.

The upper plot of Fig. 7 displays the controller temperature profile of our system, with the insert displaying the ≈80 mK temperature overshoot on an expanded scale. The cooling time clock starts when T_g is crossed, and stops when the controller has determined that T_m is reached. The total time to implement this protocol is about 90 s. However, the sample's memory is not characterized by this time, but rather by an effective cooling time t_c^{eff} derived from the peak of the relaxation function $S(t)$ for the CCP cooling protocol. The result is displayed in the lower plot of Fig. 7. The effective cooling time for this protocol is found to be $t_c^{\mathrm{eff}} \approx 70$ s. It is important to emphasize that the oscillations of T in the vicinity of T_m have a profound effect on the memory of the spin glass.[22] In this case, the effective cooling time (≈70 s), is substantially shorter than the observed time to reach T_m(≈90 s).

The TRM decay curves for the CCP cooling protocol are plotted in the upper set of curves in Fig. 8, including the ZTRM decay (the lowest curve). The lower graphs in Fig. 5 are the $S(t)$ relaxation functions for the $M_{\mathrm{TRM}}(t,t_w)$ curves.

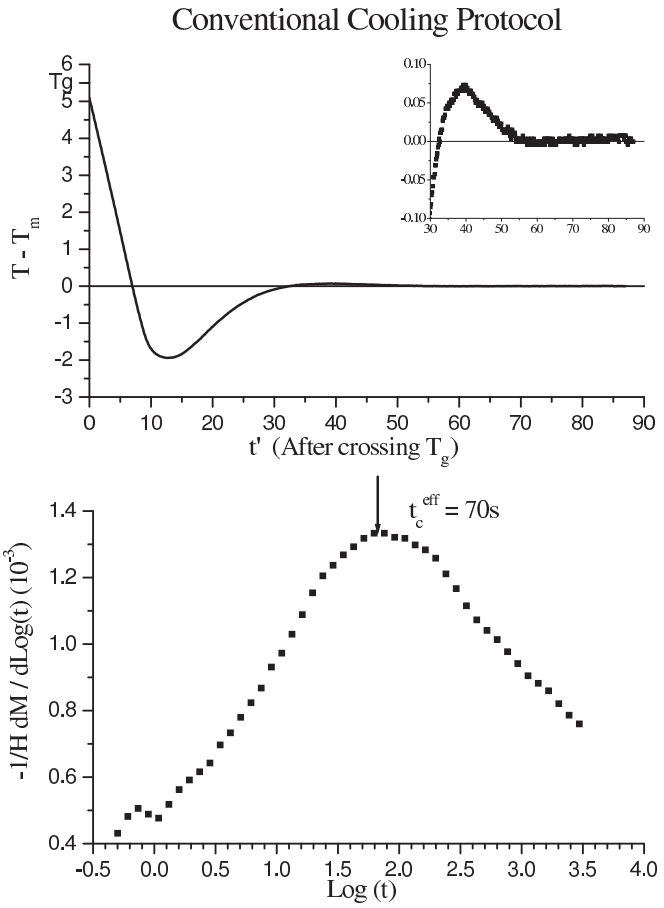

FIG. 7. CCP cooling protocol. The cooling rate is 0.6 K/s. The insert in the upper plot magnifies the temperature oscillation. The temperature rises as much as 100 mK above T_m. The lower graph is the relaxation function $S(t)$ for this cooling protocol, from which $t_c^{\rm eff} = 70$ s is extracted. The $S(t)$ curve is asymmetric, with no apparent plateau at longer time.

E. 43-s effective cooling time protocol 5—no overshoot version 1 (NOS1)

The temperature in the "conventional" cooling protocol oscillates around T_m until the temperature is stabilized (see Sec. II D). Using the computer control of the heater power, we were able to remove the oscillations, creating a "no overshoot" cooling protocol, that we designate NOS1. The protocol is illustrated in the upper plot of Fig. 9.

The cooling rate for NOS1 is the same as for CCP, 0.6 K/s. The temperature is allowed to fall 4 K below T_m. Heat is then added to the system to increase the temperature and slowly approach T_m from below. The total time, from when T_g is crossed until T_m is reached and the temperature is determined to be stable, is just over $t_c = 88$ s. The relaxation function $S(t)$ for the ZTRM is displayed on the lower plot of Fig. 9, peaking at $t_c^{\rm eff} = 43$ s, considerably shorter than for CCP where $t_c^{\rm eff} = 70$ s. This clearly illustrates the enhancement of aging caused through positive ΔT during the cooling cycle.

The TRM decay curves for the NOS1 cooling protocol are plotted in the upper set of curves in Fig. 10, including the ZTRM (the lowest curve). The lower figure displays the $S(t)$ relaxation functions for the $M_{\rm TRM}(t,t_w)$ curves.

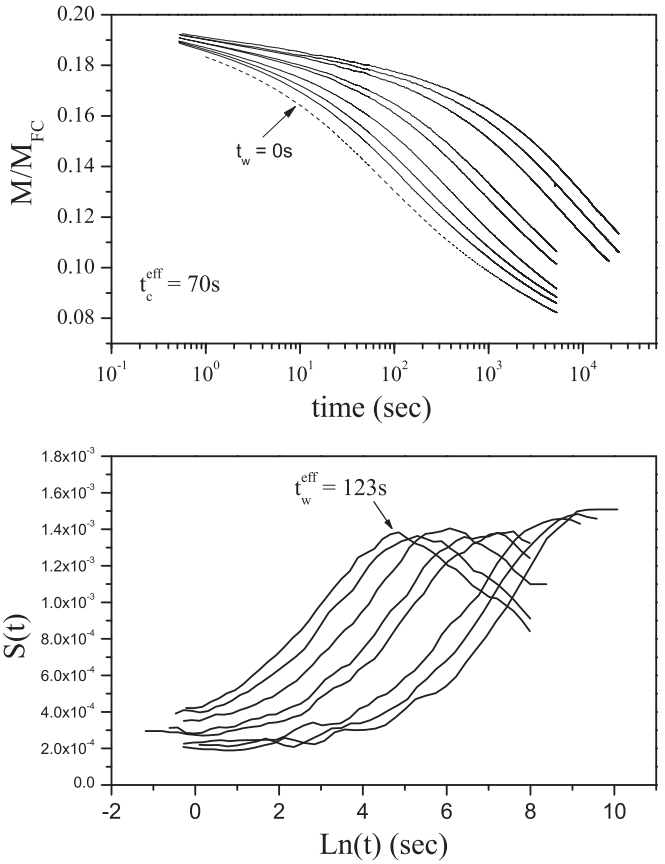

FIG. 8. $M_{\rm TRM}(t,t_w)$ decays for the CCP cooling protocol. The curves are for t_w 50, 100, 300, 630, 1000, 3600, 6310, and 10 000 s, respectively. The uppermost magnetization curve has the longest waiting time and the decay curves systematically decrease in magnitude as the waiting time decreases. The lowest decay curve (dashed line) is the ZTRM ($t_w = 0$ s). The lower figure displays the relaxation function $S(t)$ for the $M_{\rm TRM}(t,t_w)$ curves. The effective waiting time $t_w^{\rm eff} = 123$ s is extracted from the maximum of the $S(t)$ relaxation function for the $t_w = 50$ s.

F. 19-s effective cooling time protocol 6—no overshoot version 2 (NOS2)

The final protocol, having the shortest cooling time and fastest cooling rate, NOS2, is the "fast" cooling protocol, and is illustrated in the upper curve of Fig. 11. To achieve this short cooling time, the cooling rate was increased, and the time during the undershoot below T_m was minimized.

An increased amount of helium gas was added to the sample jacket and surrounding jacket in order to increase the cooling rate. However, the increased cooling rate was accompanied by greater thermal noise, as increased heater power was necessary to sustain the measuring temperature. For the NOS2 protocol, the temperature instability increased from 5 to 10 mK.

The temperature was lowered below T_m in NOS2 with the faster cooling rate, falling ≈1 K below T_m, less than the NOS1 Protocol (≈3.5 K). With this smaller ΔT, the rise to T_m was more rapid than for NOS1. Another important feature of NOS2 is the time required for thermal equilibration. NOS2 minimizes the equilibration time: once the temperature has reached T_m, the protocol is ended and the magnetic field removed. The cooling profile and ZTRM decays were measured several

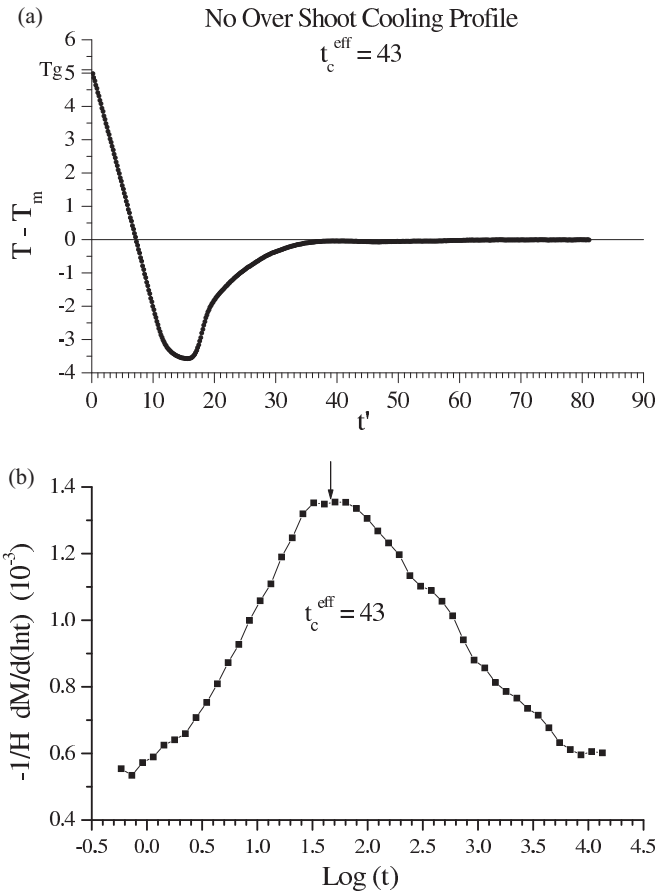

FIG. 9. NOS1 cooling protocol. The cooling rate is 0.6 K/s. The temperature falls 4 K below T_m, then slowly raised to T_m from below, and not allowed to increase above T_m. The lower figure is the relaxation function $S(t)$ for this cooling protocol, from which $t_c^{\rm eff} = 43$ s is extracted.

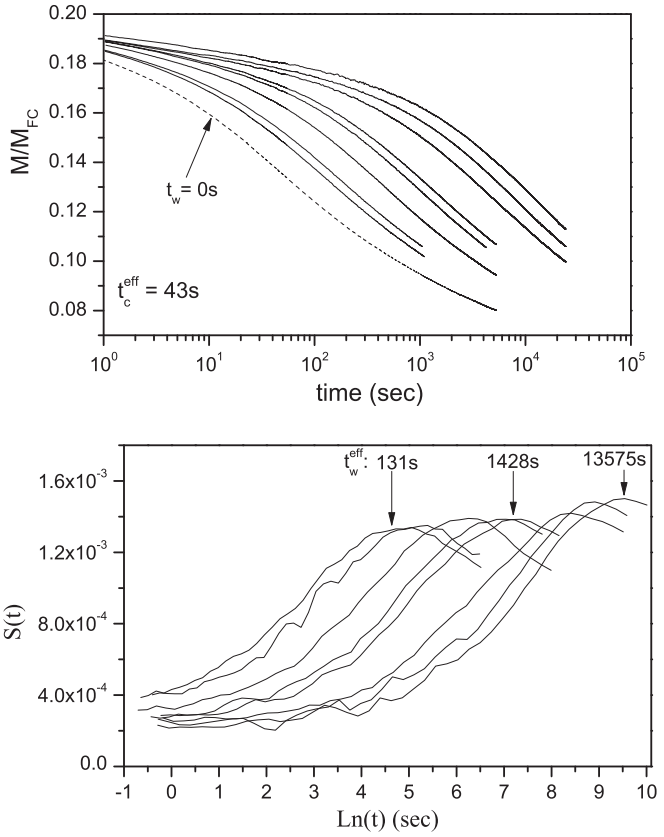

FIG. 10. $M_{\rm TRM}(t,t_w)$ decays for the NOS1 cooling protocol. The curves are for t_w 50, 100, 300, 630, 1000, 3600, 6310, and 10 000 s, respectively. The uppermost magnetization curve has the longest waiting time and the decay curves systematically decrease in magnitude as the waiting time decreases. The lowest decay curve (dashed line) is the ZTRM ($t_w = 0$). The lower figure displays the relaxation function $S(t)$ for the $M_{\rm TRM}(t,t_w)$ curves. The effective waiting time $t_w^{\rm eff} = 131$ s is extracted from the maximum of the $S(t)$ relaxation function for the $t_w = 50$ s.

times, before, during, and after the TRM decays to ensure reproducibility. The NOS2 protocol generated the shortest $t_c^{\rm eff}$ for all of the protocols, ≈19 s.

The TRM decay curves for the NOS2 cooling protocols are plotted in the upper set of curves in Fig. 12. The lower figure displays the $S(t)$ relaxation function for the $M_{\rm TRM}(t,t_w)$ curves. Importantly, the $t_w^{\rm eff}$ for NOS2 are roughly comparable to the actual t_w. This observation will form the basis for analysis in the following section.

III. SCALING ANALYSIS

Six different cooling protocols were exhibited in Sec. II for arriving at the measuring temperature, $T_m = 0.83T_g$. The first two protocols (NUS1, NUS2) approached T_m from above with no undershoot. The third protocol (NUS3) approached T_m from above with only a slight undershoot. The fourth protocol (CCP) is more like the "standard" cooling protocol, typical of commercial magnetometers, where the temperature approached T_m with a decaying oscillation around the final value. The last two protocols (NOS1, NOS2) undershoot T_m, approaching from below with no overshoot. The work of Refregier *et al.*,[19] Lederman *et al.*[20] and Hammann *et al.*,[20] interpret the spin glass transition as a continuous set of phase transitions, beginning at T_g and extending to the lowest temperatures accessible within the time window of the experiments.[20] From Ref. 31, "... when heating a spin-glass from zero temperature up to T_g, we go through a series of micro phase transitions characterized by the melting of two or more states into one state at a higher temperature." From Ref. 32, "... in contrast to the simple bifurcation at T_c, which is observed in conventional second-order phase transitions..., the spin glass behavior might correspond somehow to a *continuous* sequence of bifurcations just starting at T_g. In particular ... the minima, to which the bifurcfations lead, should be different in height, which implies the appearance of metastability." Finally, from Ref. 33, "We conceive of the spin-glass displaying broken ergodicity in which a sequence of bifurcations leads to many mutually inaccessible ... regions of configuration space as the temperature is lowered ... We tentatively suggest that a spin-glass is critical everywhere in the ordered region of the phase diagram."

As a result, the temperature quench for spin glasses is a complicated process. Within the range of ≈0.3 K for our sample [Cu:Mn (6 at.%), $T_m = 26$ K, $T_g = 31.5$ K], aging occurs more rapidly for temperatures just above the measuring

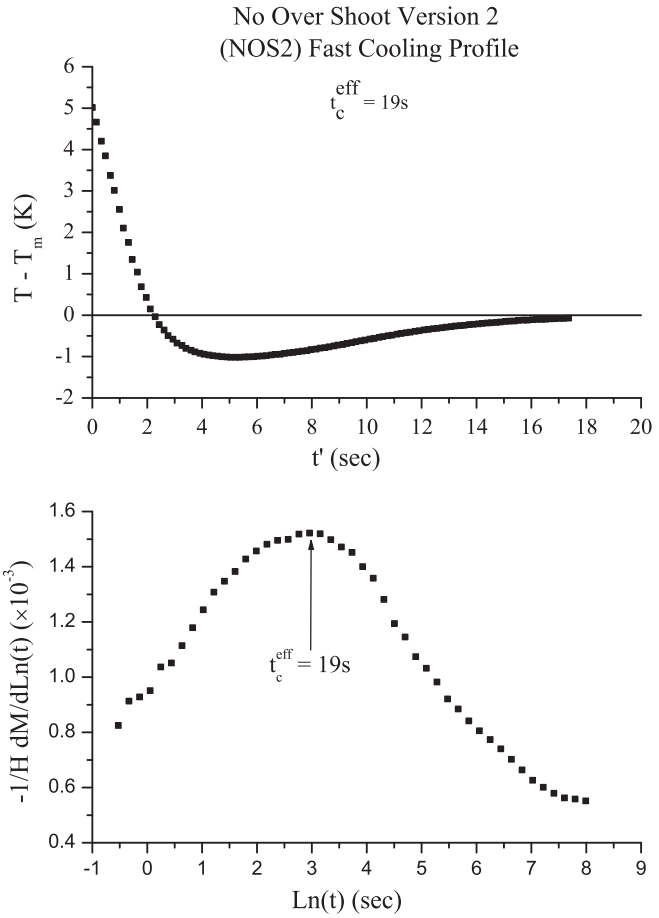

FIG. 11. NOS2 cooling protocol. This is the fastest cooling protocol. The cooling rate has been increased to 1 K/s, and the temperature only falls 1 K below T_m. No additional time is added for equilibration. The lower graph is the relaxation function $S(t)$ for this cooling protocol, from which $t_c^{\rm eff} = 19$ s is extracted. There is a rapid fall in $S(t)$ after the peak, and the curve remains asymmetric.

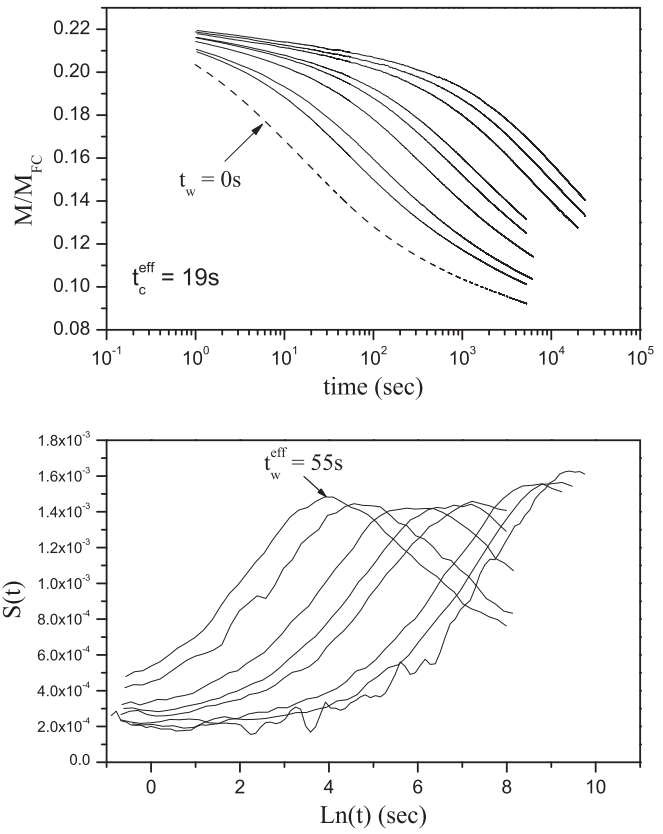

FIG. 12. $M_{\rm TRM}(t,t_w)$ decays for the NOS2 "fast" cooling protocol. The curves are for t_w 50, 100, 300, 630, 1000, 3600, 6310, and 10 000 s, respectively. The uppermost magnetization curve has the longest waiting time and the decay curves systematically decrease in magnitude as the waiting time decreases. The lowest decay curve is the ZTRM ($t_w = 0$ s). The lower figure displays the relaxation functions $S(t)$ for the $M_{\rm TRM}(t,t_w)$ curves. The effective time $t_w^{\rm eff} = 55$ s is extracted from the maximum of the $S(t)$ relaxation function for $t_w = 50$ s.

temperature or more slowly for temperatures just below the measuring temperature. As shown in Sec. II, in the small temperature interval $\Delta T \approx 300$ mK in the immediate vicinity of T_m, aging decreases *reversibly* for negative temperature shifts, while aging accelerates for positive temperature shifts. Above this narrow interval, the decay curves do not return to those at T_m upon cycling for these larger positive temperature shifts.

All of the TRM magnetization decays, when viewed on a logarithmic scale, have a maximum rate of decay producing a peak in $S(t)$ at a time that we designate as $t_w^{\rm eff}$. The effective time for reaching T_m, $t_c^{\rm eff}$ is found to always be less than the respective $t_w^{\rm eff}$. This is associated more rapid diffusion caused by decreases in the (strongly temperature dependent) barrier heights.

The $t_w^{\rm eff}$ times derived from the peak of the relaxation function $S(t)$ as a function of Log(t) for the three no undershoot cooling protocols are listed in Table I at the different effective cooling times $t_c^{\rm eff}$. Similarly, Table II lists the $t_w^{\rm eff}$ times for the "conventional," the no overshoot, and the fastest cooling protocols. The $t_w^{\rm eff}$ were extracted from fitting an eighth order polynomial to the relaxation function $S(t)$ curves. The latter were "filtered" into equally spaced Log(t) time increments. Using 50 points to fit to $S(t)$, the time where the first derivative of $S(t)$ crosses zero was taken as the peak position for $S(t)$ as a function of t. Whenever possible, several $t_w^{\rm eff}$'s were averaged.

TABLE I. TRM effective waiting times $t_w^{\rm eff}$ for the three cooling protocols with the largest effective cooling times.

	$t_w^{\rm eff}$ (s)		
t_w	NUS1 $t_c^{\rm eff} = 406$ s	NUS2 $t_c^{\rm eff} = 143$ s	NUS3 $t_c^{\rm eff} = 105$ s
50	465 ± 36	251 ± 7	192 ± 6
100	483 ± 40	305 ± 8	250 ± 3
300	719 ± 43	546 ± 31	465 ± 24
630	1137 ± 92	915 ± 48	1038 ± 200
1000	2096 ± 236	1443 ± 50	1640 ± 318
3600	5663 ± 382	5936 ± 844	5805 ± 737
6310	9021 ± 618	7616 ± 284	7744 ± 494
10 000	12 910 ± 1591	13 901 ± 670	14 605 ± 370

TABLE II. TRM effective waiting times t_w^{eff}, for the "conventional," the no overshoot, and the fastest cooling protocols, leading to the shortest effective cooling times, t_c^{eff}. Even for the fastest cooling protocol, $t_w^{\text{eff}} > t_w$.

	t_w^{eff} (s)		
	CCP	NOS1	NOS2
t_w	$t_c^{\text{eff}} = 70$ s	$t_c^{\text{eff}} = 43$ s	$t_c^{\text{eff}} = 19$ s
50	123 ± 4	131 ± 10	55 ± 5
100	205 ± 5	171 ± 19	115 ± 10
300	409 ± 80	502 ± 20	379 ± 15
630	993 ± 36	1046 ± 5	915 ± 50
1000	1655 ± 20	1428 ± 20	1409 ± 50
3600	6141 ± 350	4503 ± 155	5822 ± 200
6310	8101 ± 792	7586 ± 80	8541 ± 200
10 000	12 596 ± 1328	13 575 ± 459	14 030 ± 200

Relaxation functions $S(t)$ for each of the six cooling protocols are plotted against Log(t) for each of the eight waiting times in Tables I and II and in Fig. 13. A vertical line is drawn at $t = t_w$ for guidance. As seen in the figure, $t_w^{\text{eff}} > t_w$ for every curve, regardless of the cooling protocol. Curves with $t_w = 50$, 100, 300, and 630 s systematically display an increasing shift in the peak position (towards t_w) with decreasing effective cooling times t_c^{eff}. For the shortest

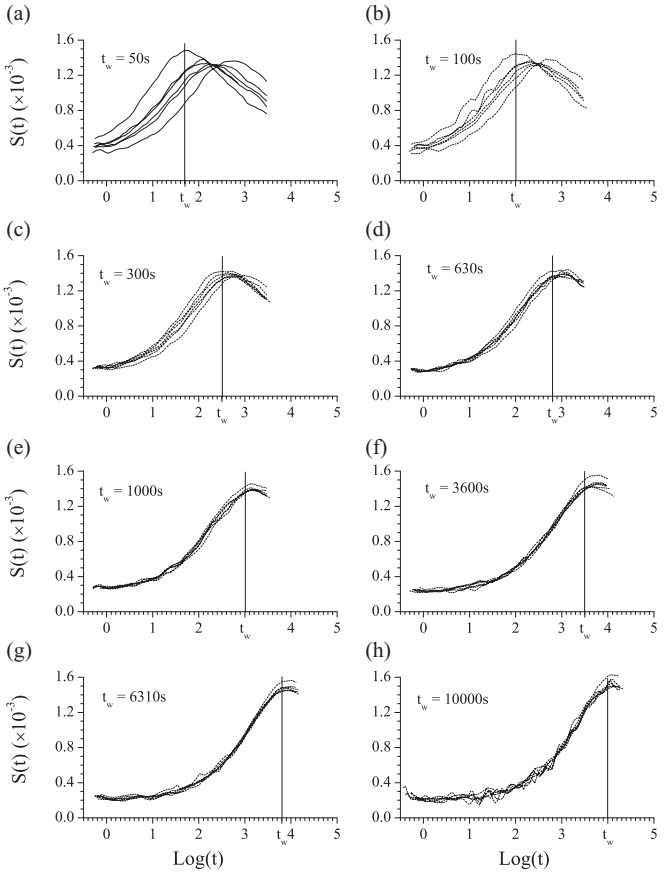

FIG. 13. Relaxation functions $S(t)$ for the different cooling protocols at specific t_w. When $t_w > 1000$ s, the cooling protocol becomes irrelevant.

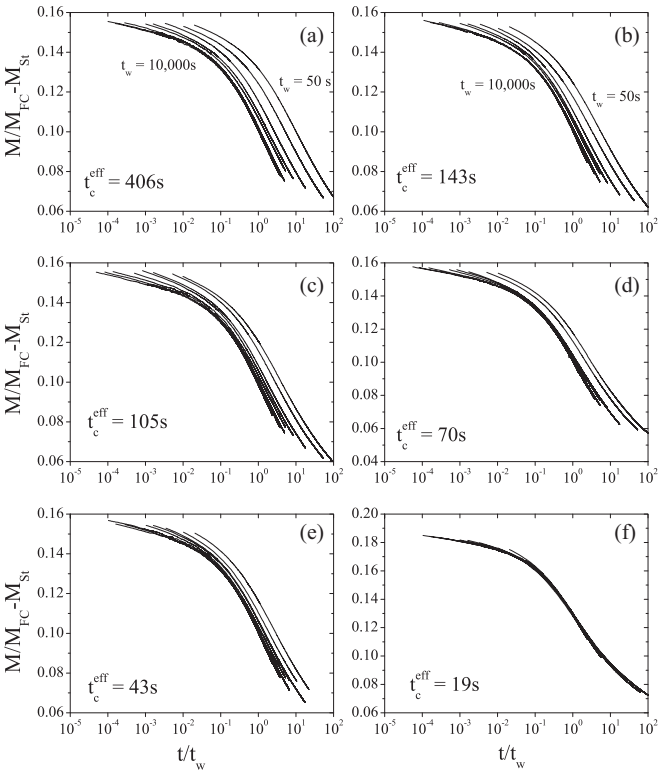

FIG. 14. Scaling of TRM decay curves with the stationary part subtracted. There is an improvement in scaling at the short times. We use $\alpha = 0.02$ and $A = 0.06$ from Ref. 5 and the attempt time $\tau = 10^{-12}$ from Ref. 36.

t_c^{eff}, the fast cooling protocol, the peak in $S(t)$ lies closest to t_w ($t_w^{\text{eff}} = 55 \pm 5$ s at $t_w = 50$ s). For the longer waiting times, $t_w = 1000$, 3600, 6310, and 10 000 s, the $S(t)$ curves in Fig. 13 are less affected by t_c^{eff}, but continue to peak at times $t > t_w$.

Plots of the decays of $M_{\text{TRM}}(t,t_w)$ less the stationary part defined in Eqs. (4) and (5) and scaled as t/t_w and as λ/t_w^{μ} [$\lambda = t_e$ in Eq. (1)], respectively, are exhibited in Figs. 14 and 15 for each of the six cooling protocols. Perfect scaling is not observed [the effect of subtraction of the stationary term, (4) and (5), will be discussed later in this section]. In general, for either scaling, the longer the effective cooling time, the larger the spread of the curves. Plots A in both figures are indicative of a cooling time comparable to the quantum design magnetic properties measurement system at the University of California, San Diego.[18] Our results are similar: the longer the cooling time, the greater the spread of the TRM decay curves. As the cooling time decreases, the TRM decay curves begin to collapse onto one another for both t/t_w and λ/t_w^{μ} scaling.

From Fig. 14, the t/t_w scaled TRM decay curve with the largest t_w (10 000 s) lies below the shorter t_w curves. It also appears that the higher t_w curves decay faster than the smaller t_w. This effect is well known and is referred to as "subaging."[14,18,21]

Figure 15 introduces λ/t_w^{μ} scaling[15–17] into the time dependence of the TRM decay. The plots are arranged from the longest t_c^{eff} [see Fig. 15(a)] to the shortest t_c^{eff} [see Fig. 15(f)]. It is seen that μ approaches unity as t_c^{eff} is reduced. For the longest t_c^{eff} in Fig. 15, 406 s, $\mu \approx 0.88$. This value of μ is

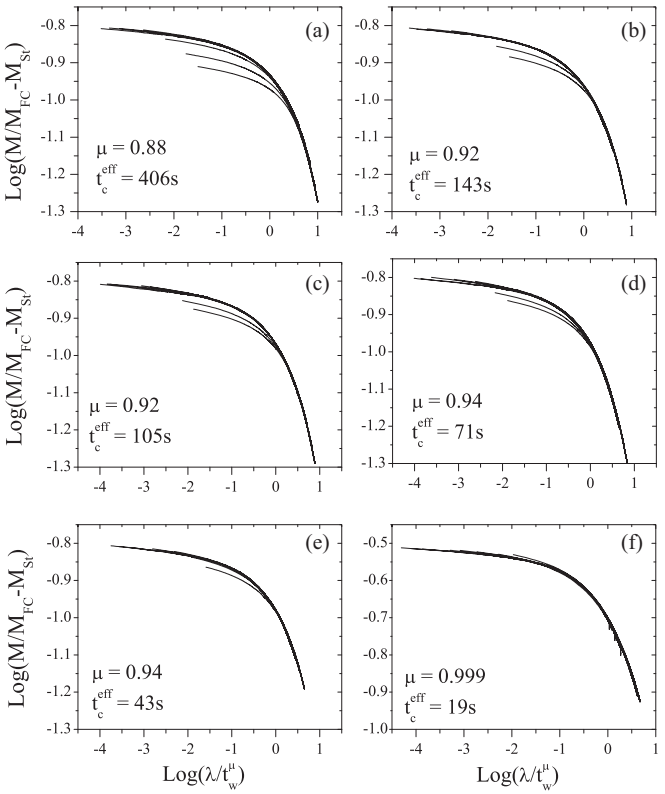

FIG. 15. μ scaling of TRM decay curves with the stationary term subtracted. Subtraction of the stationary term slightly increases the value of μ, but it remains less than one.

roughly consistent with previous work for the same reduced temperature. What is not the same is the behavior of μ as $t_c^{\rm eff}$ is reduced. From Fig. 15, it is clear that μ begins to approach unity rapidly as $t_c^{\rm eff}$ is reduced, approximating 0.999 for the shortest $t_c^{\rm eff} = 19$ s.

As discussed earlier in this paper, the stationary term, (4) and (5), should be subtracted from our results before a final analysis is attempted. Because $\chi''(\omega,t)$ measurements are not practical for metallic samples, we make use of the value of A and α from Vincent *et al.*[29] for the (low anisotropy) sample Ag:Mn. They find $\alpha = 0.02$ with $A = 0.1$. In our case, we used their value for α, but the coefficient A was chosen so that the scaling was improved for the "conventional" ($t_c^{\rm eff} = 406$ s) cooling protocol ($A = 0.06, \tau = 10^{-12}$ s). The same stationary term was then subtracted from all the TRM decay data, regardless of cooling protocol. There is some improvement in scaling at shorter times, $t < t_w$, but no significant improvement at longer times. The resulting TRM decays, scaled with t/t_w, are plotted in Fig. 14.

In order to make contact with λ/t_w^{μ} scaling,[15–17] the TRM decays, less the stationary term, are also displayed in Fig. 15. It is important to note that, for our "conventional" cooling protocol, $t_c^{\rm eff} = 406$ s, $\mu = 0.88$. As $t_c^{\rm eff}$ shortens, μ increases, rising at $t_c^{\rm eff} = 19$ s to $\mu = 0.999$. Vincent *et al.*[29] find for (low anisotropy) Ag:Mn, $\mu = 0.97$ upon subtraction of the stationary term. That the result for Ag:Mn lies within the observed range for Cu:Mn suggests that $\mu \to 1$ for Ag:Mn as well as Cu:Mn for sufficiently short $t_c^{\rm eff}$.

IV. DISCUSSION

Aging is found for many systems far from equilibrium.[34,35] Spin glasses are important examples because their temporal behavior can be affected through magnetic field and temperature variations. In addition to their intrinsic theoretical interest, we believe that one can learn a great deal about the behavior of nonlinear complex system dynamics from a study of this prototypical example. In this paper, we have examined the dependence of the spin glass time dependent response as a function of the initial preparation of the system through changes in cooling protocols from the glass temperature T_g to the measurement temperature T_m.

The spin glass transition temperature T_g can be thought of as the temperature at which the first finite barrier diverges as the system is cooled. From that point on, within the time domain available to our experiments, there is a continuous growth to infinity of barrier heights as the temperature continues to decrease below T_g. This "carves up" phase space into regions separated from one another by infinite barriers. These regions are self similar with one another, so that the dynamics remain the same within each region as the temperature is lowered.

The temperature dependence of the barrier heights underpins the interpretation of our experiments. It is the basis for scaling approaching t/t_w as $t_c^{\rm eff}$ is reduced (equivalent to μ approaching unity). As the spin glass is cooled to within ΔT above T_m, the barriers are lower than those at T_m, and within the same time window, the spin glass can explore barriers of concomitant height to those explored at T_m. As the temperature then returns to T_m, these barriers grow in height,[20] so that *it appears* as though the system has explored higher barriers that would have been explored within the same time interval at T_m. The barrier heights are related to the spin glass correlation length through the relationship[36]

$$\Delta\left(t_c^{\rm eff},T\right)/k_\beta T_g = 6\left[\ln\xi\left(t_c^{\rm eff},T\right) + 0.44\right]. \qquad (6)$$

The larger $t_c^{\rm eff}$, the larger the highest occupied barrier at T_m, and the greater the correlation length $\xi(t_c^{\rm eff},T)$. This relationship was anticipated by Koper and Hilhorst,[37] as well as by Rieger[38] and Sibani *et al.*[39] As seen from Eq. (6), the larger $t_c^{\rm eff}$, the larger the highest occupied barrier at T_m, and the greater the correlation length $\xi(t_c^{\rm eff},T)$.

In light of the structure of the sample, we hypothesize that the effect of $t_w^{\rm eff}$ on μ arises from the end of aging when $\xi(t_c^{\rm eff},T)$ is of the order of the length scale of a given crystallite[21,40,41] comprising the Cu:Mn sample.[42] Beyond that time, an individual crystallite relaxes exponentially in time with the highest barrier from (6) determining the rate of relaxation. Averaging the exponential over a distribution of crystallites yields a logarithmic time dependence.[43,44] The decay of $M_{\rm TRM}(t,t_w)$ will be a combination of contributions from crystallites that continue to age and those for which aging has ceased. This is accommodated through scaling the decay of $M_{\rm TRM}(t,t_w)$ with $\mu \neq 1$.

It is important to distinguish between the correlation length at the effective cooling time, $t_c^{\rm eff}$, and at the time during the measurement of the decay of the TRM. If $\xi(t_c^{\rm eff},T)$ is larger than the crystallite size, then when the magnetic field

is removed, that crystallite will decay exponentially in time with a barrier height given by (6). If $\xi(t_c^{\rm eff},T)$ is smaller than the crystallite size, when the magnetic field is removed, $\xi(t,T)$ will continue to grow until $\xi(t_c^{\rm eff}+t,T)$ equals the crystallite size. The TRM for that crystallite will then cross over from conventional TRM time decay to exponential time decay. If the sample contains a distribution of crystallite sizes that overlaps both regimes, the TRM decay will not scale as t/t_w. This lack of scaling is accommodated by fitting the TRM decay with an empirical parameter $\mu < 1$ as defined in Eqs. (2) and (3). If, however, $\xi(t_c^{\rm eff},T)$ is less than the size of any of the sample crystallites, perfect scaling obtains, and $\mu = 1$ as long as $\xi[(t_c^{\rm eff}+t),T]$ remains less than crystallite sizes. The situation for our sample of Cu:Mn (6 at.%) will be analyzed below in this context.

For our sample, Rodriguez[42] finds a distribution of small crystallites, with diameters extending from 80 to 300 nm, and an average diameter of 100 nm, in between longer single crystals of an average width of 660 nm. Reference 22 demonstrates that for the shortest $t_c^{\rm eff} = 7$ s, a crossover to logarithmic decay takes place at $t_c^{\rm eff} \approx 10^3$ s. This is interpreted to be a consequence of $\xi(t_c^{\rm eff} = 10^3,T) \sim 100$ nm. For the NUS1 cooling protocol, $t_c^{\rm eff} = 406$ s, so that on a relative scale $\xi \sim 87$ nm. Aging would have terminated on some of the smaller crystallites, and our hypothesis would lead us to $\mu < 1$.

As $t_c^{\rm eff}$ shortens, Fig. 15 demonstrates that $\mu \to 1$. A consistency check is to take the shortest $t_c^{\rm eff} = 19$ s and calculate $\xi(t_c^{\rm eff} = 19, T_m)$. We find, on a relative scale, $\xi(t_c^{\rm eff} = 19\ {\rm s}, T_m) = 54$ nm, well short of the smallest estimated crystallite size.[42] The intermediate values for $t_c^{\rm eff}$ contained in Tables I and II cross over into length scales $\xi(t_c^{\rm eff})$ that encompass the smaller crystallites. We estimate that a lower boundary for cross over occurs when $\xi(t_c^{\rm eff},T_m) \approx 80$ nm, yielding $t_c^{\rm eff} \approx 237$ s. From Fig. 15, this time is intermediate between measurements where $\mu = 0.88$ (curve A, with $t_c^{\rm eff} = 406$ s) and where it begins to increase to $\mu = 0.92$ (curve B, with $t_c^{\rm eff} = 143$ s). Figure 15 demonstrates that, as $t_c^{\rm eff}$ shortens, so that $\xi(t_c^{\rm eff},T_m)$ becomes progressively smaller than the smallest crystallite, $\mu \to 1$ as hypothesized.

It is interesting to note that, because of the small exponent in the expression for $\xi(t_c^{\rm eff},T)$ in Ref. 36, even the shortest $t_c^{\rm eff}$ in our measurements, 19 s, leads to a relative correlation length for our sample of 54 nm. This means that for samples with large numbers of small crystallites, a cross over to logarithmic behavior during aging can take place, and in our analysis, values of $\mu < 1$. This may have relevance to measurements on other spin glasses.

It is important to make reference to the work of Parker *et al.*[45] They explored the effect of cooling rates on aging processes in three "well-characterized spin glasses, $CdCr_{1.7}In_{0.3}S_4$, Au:$Fe_{8\%}$, and $Fe_{0.5}Mn_{0.5}TiO_3$." They were able to achieve, using a Cryogenics S600 SQUID magnetometer, rapid cooling that reduced the peak time for $S(t)$ to 14 s for $CdCr_{1.7}In_{0.3}S_4$, and 45 s for $Fe_{0.5}Mn_{0.5}TiO_3$. Upon subtraction of the stationary part, they found $\mu = 0.91$ and 0.84, respectively, while slower cooling protocols gave smaller values for μ. They proposed a mechanism to account for the discrepancy between our results reported above and their results, associated with "subtle temperature variations during the first few tens of seconds of t_w, which are in turn influenced by the cooling protocol."

TABLE III. Values of the freezing temperature T_g, and the ratio of anisotropy constant (in erg/mol of magnetic sites) to T_g. Reproduced from Ref. 46.

Sample	$T_g(K)$	$K(0)/T_g \times 10^{-5}$
CuMn 3%	18.5	0.068
AgMn 3%	11.9	0.16
$CdCr_2InS_4$	16.8	0.8
AuFe 8%	23.9	1.32
$(Fe_{0.1}Ni_{0.9})_{75}P_{16}B_6Al_3$	13.4	2.65

We suggest a different reasoning, associated with the "Ising-like" characteristics of their samples as compared to Ag:Mn[29] (where μ was found to be $\sim$0.97 after subtraction of the stationary term) and Cu:Mn (this paper, where μ is found to approach unity). Torque measurements by Petit *et al.*[46] found a hierarchy of anisotropies for spin glasses (their Table I is reproduced here as Table III). Of the three samples considered by Parker *et al.*,[45] only two were included in the work of Petit *et al.*:[46] Au:Fe (8 at.%) and $CdCr_{1.7}In_{0.3}S_4$. Petit *et al.* also included Ag:Mn (3 at.%) and Cu:Mn (3 at.%). We have listed these four compounds in order of decreasing anisotropy. Setting their $K(0)/T_g \times 10^{-5}$ equal to unity for the least anisotropic material, Cu:Mn, one finds the ratios 19.4, 11.8, 2.4, 1 for the relative anisotropies.

Anisotropies can play a pivotal role in aging. For example, Dupuis *et al.*[47] state: "In the Ising sample, the contribution of aging at low temperature to aging at a slightly higher temperature is much *larger* than expected from thermal slowing down. This is at variance with the behavior observed until now in other spin glasses, which show the opposite trend of a free-energy barrier growth as the temperature is decreased." Bert *et al.*[48] find "... the extracted coherence length is noticeably smaller in the Ising sample ... but grows faster with time." The former finding is most troubling when comparing Parker *et al.*[45] with our own work, for it *reverses* the effect of cycling in the vicinity of T_m. Finally, there was no reference to the distribution of crystallite sizes in the work of Parker *et al.*[45] Given the small exponent in the expression for $\xi(t_w,T)$, even relatively short t_w can give rise to length scales of the order of $\approx 80a_0$, where a_0 is the average spacing between magnetic sites. It is then possible that the effects described above might be the origin of their values of $\mu < 1$.

In conclusion, we have examined the dynamical behavior of spin glasses under different initial state preparation conditions. We have shown how sensitive the response to changes in magnetic field are to the cooling profile for arriving at the measuring temperature T_m. We have made quantitative the explanation for the approach to t/t_w scaling as the cooling protocol minimizes the time spent immediately above T_m. It would be of great interest to explore thin film spin glasses to see the cross over from three to two dimensional behavior as the correlation length $\xi(t_w,T)$ grows to the thin film thicknesses.

ACKNOWLEDGMENTS

The authors are indebted to G. A. Henkelman, D. E. Markov, and P. J. Rossky for discussions concerning glassy dynamics, an extensive conversation on correlations in glasses with D. R. Reichman, and detailed correspondence with F. Ritort. The authors would also like to thank P. Sibani for stimulating discussions on aging models. We wish to thank S. Guchhait for the preparation of the figures in this paper. This research was supported in part by the Cockrell Family Regents Chair in Engineering at The University of Texas at Austin.

[1] V. Cannella and J. A. Mydosh, Phys. Rev. B **6**, 4220 (1972).

[2] H. Maletta, W. Felsch, and J. L. Tholence, J. Magn. Magn. Mat. **9**, 41 (1978)

[3] See, for example, K. Binder and A. P. Young, Rev. Mod. Phys. **58**, 810 (1986), and references therein.

[4] C. Djurberg, K. Jonason, and P. Nordblad, Eur. Phys. J. B **10**, 15 (1999).

[5] Ph. Refregier, M. Ocio, J. Hammann, and E. Vincent, J. Appl. Phys. **63**, 4343 (1988).

[6] N. Bontemps and R. Orbach, Phys. Rev. B **37**, 4708 (1988).

[7] D. E. MacLaughlin, L. C. Gupta, D. W. Cooke, R. H. Heffner, M. Leon, and M. E. Schillaci, Phys. Rev. Lett. **51**, 927 (1983).

[8] F. Mezei and A. P. Murani, J. Mag. Mag. Mat. **14**, 211 (1979).

[9] H. Alloul and P. Mendels, Phys. Rev. Lett. **54**, 1313 (1985).

[10] R. V. Chamberlin, M. Hardiman, and R. Orbach, J. Appl. Phys. **52**, 1771 (1983).

[11] L. Lundgren, P. Svedlindh, P. Nordblad, and O. Beckman, Phys. Rev. Lett. **51**, 911 (1983); J. Appl. Phys. **57**, 3371 (1985).

[12] P. Nordblad, P. Svedlindh, L. Lundgren, and L. Sandlund, Phys. Rev. B **33**, 645 (1986).

[13] P. Nordblad, P. Svedlindh, L. Sandlund, and L. Lundgren, Phys. Lett. A **120**, 475 (1987).

[14] L. C. E. Struik, *Physical Aging in Amorphous Polymers and Other Material* (Elsevier, Houston, 1978).

[15] M. Ocio, M. Alba, and J. Hammann, J. Phys. (Paris) Lett. **46**, L1101 (1985).

[16] M. Alba, M. Ocio, and J. Hammann, Euro. Phys. Lett. **2**, 45 (1986).

[17] M. Alba, J. Hammann, M. Ocio, and Ph. Refregier, J. Appl. Phys. **61**, 3683 (1987).

[18] V. S. Zotev, G. F. Rodriguez, G. G. Kenning, R. Orbach, E. Vincent, and J. Hammann, Phys. Rev. B **67**, 184422 (2003).

[19] Ph. Refregier, E. Vincent, J. Hammann, and M. Ocio, J. Phys. (France) **48**, 1533 (1987).

[20] M. Lederman, R. Orbach, J. M. Hammann, M. Ocio, and E. Vincent, Phys. Rev. B **44**, 7403 (1991); J. Hammann, M. Lederman, M. Ocio, R. Orbach, and E. Vincent, Physica (Amsterdam) **185A**, 278 (1992).

[21] G. F. Rodriguez, G. G. Kenning, and R. Orbach, Phys. Rev. Lett. **91**, 037203 (2003).

[22] G. G. Kenning, G. F. Rodriguez, and R. Orbach, Phys. Rev. Lett. **97**, 057201 (2006).

[23] G. G. Kenning, J. Bowen, P. Sibani, and G. F. Rodriguez, Phys. Rev. B **81**, 014424 (2010).

[24] P. Sibani and G. G. Kenning, Phys. Rev. E **81**, 011108 (2010).

[25] D. S. Fisher and D. A. Huse, Phys. Rev. B **38**, 373 (1988); **38**, 386 (1988).

[26] P. Sibani, J. C. Schön, P. Salamon, and J.-O. Andersson, Europhys. Lett. **22**, 479 (1993); P. Sibani and P. Schriver, Phys. Rev. B **49**, 6667 (1994); J. C. Schön and P. Sibani, Europhys. Lett. **49**, 196 (2000).

[27] R. Richert, Phys. Rev. Lett. **104**, 085702 (2010).

[28] R. V. Chamberlin, Phys. Rev. Lett. **83**, 5134 (1999).

[29] E. Vincent, J. Hammann, M. Ocio, J.-P. Bouchaud, and L. F. Cugliandolo, S*low Dynamics and Aging in Spin Glasses* in Complex Behaviour of Glassy Systems, Proceedings of the XIV Sitges Conference, Sitges, Barcelona, Spain, 10–14 June, 1996, edited by M. Rubi and C. Perez-Vicente, Lect. Notes Phys. 492 (Springer, Berlin, 1997).

[30] G. G. Kenning, D. Chu, and R. Orbach, Phys. Rev. Lett. **66**, 2923 (1991).

[31] M. Mezard, G. Parisi, N. Sourlas, G. Toulouse, and M. Virasoro, J. Phys. (France) **45**, 843 (1984).

[32] U. Krey, J. Magn. Magn. Mat. **6**, 27 (1977).

[33] F. T. Bantilan Jr. and R. G. Palmer, J. Phys. **F 11**, 261 (1981)

[34] See, for example, M. Henkel, and M. Pleimling, *Non-Equilibrium Phase Transitions Volume 2: Ageing and Dynamical Scaling Far from Equilibrium Series*, Theoretical and Mathematical Physics (Springer, Berlin, 2010), and references therein.

[35] A. Amir, S. Borini, Y. Oreg, and Y. Imry, Phys. Rev. Lett. **107**, 186407 (2011).

[36] Y. G. Joh, R. Orbach, G. G. Wood, J. Hammann, and E. Vincent, Phys. Rev. Lett. **82**, 438 (1999).

[37] G. J. M. Koper and H. J. Hilhorst, J. Phys. (Paris) **49**, 429 (1988).

[38] H. Rieger, J. Phys. A **26**, L615 (1993); H. Rieger, B. Steckemetz, and M. Schreckenberg, Europhys. Lett. **27**, 485 (1994).

[39] P. Sibani and J.-O. Andersson, Physica (Amsterdam) **206A**, 1 (1994).

[40] J.-P. Bouchaud, E. Vincent, and J. Hammann, J. Phys. I **4**, 139 (1994).

[41] Y. G. Joh, R. Orbach, G. G. Wood, J. M. Hammann, and E. Vincent, J. Phys. Soc. Jpn. Suppl. A **69**, 215 (2000).

[42] G. F. Rodriguez, Thesis, University of California, Riverside, 2004.

[43] S. Guchhait, G. G. Kenning, R. Orbach, and G. Rodriguez (unpublished).

[44] S. K. Ma, Phys. Rev. B **22**, 4484 (1980); G. Mihàly and L. Mihàly, Phys. Rev. Lett. **52**, 149 (1984).

[45] D. Parker, F. Ladieu, J. M. Hammann, and E. Vincent, Phys. Rev. B **74**, 184432 (2006).

[46] D. Petit, L. Fruchter, and I. A. Campbell, Phys. Rev. Lett. **88**, 207206 (2002).

[47] V. Dupuis, E. Vincent, J. P. Bouchaud, J. M. Hammann, A. Ito, and H. A. Katori, Phys. Rev. B **64**, 174204 (2001).

[48] F. Bert, V. Dupuis, E. Vincent, J. M. Hammann, and J.-P. Bouchaud, Phys. Rev. Lett. **92**, 167203 (2004).